Supporting information (SI): Enhanced daytime secondary aerosol formation driven by gas-particle partitioning in downwind urban plumes

Mingfu Cai[1,2,3], Ye Chenshuo[4], Bin Yuan[2,3*], Shan Huang[2,3], E Zheng[2,3], Suxia Yang[5], Zelong Wang[2,3], Yi Lin[2,3], Tiange Li [2,3], Weiwei Hu[6], Wei Chen[6], Qicong Song[2,3], Wei Li[2,3], Yuwen Peng[2,3], Baoling Liang[7], Qibin Sun[7], Jun Zhao[7], Duohong Chen[8], Jiaren Sun[1], Zhiyong Yang[9], Min Shao[2,3]

[1]Guangdong Province Engineering Laboratory for Air Pollution Control, Guangdong Provincial Key Laboratory of Water and Air Pollution Control, South China Institute of Environmental Sciences, MEE, Guangzhou, Guangdong 510655, China

[2]Institute for Environmental and Climate Research, Jinan University, 51143, Guangzhou, China

[3]Guangdong-Hongkong-Macau Joint Laboratory of Collaborative Innovation for Environmental Quality, Guangzhou, China

[4] Guangdong Provincial Academy of Environmental Science, Guangzhou, 510045, China

[5] Guangzhou Research Institute of Environment Protection Co.,Ltd, Guangzhou 510620, China

[6]State Key Laboratory of Organic Geochemistry and Guangdong Key Laboratory of Environmental Protection and Resources Utilization, Guangzhou Institute of Geochemistry, Chinese Academy of Sciences, Guangzhou 510640, China

[7]School of Atmospheric Sciences, Guangdong Province Key Laboratory for Climate Change and Natural Disaster Studies, and Institute of Earth Climate and Environment System, Sun Yat-sen University, Zhuhai, Guangdong 519082, China

[8]Guangdong Environmental Monitoring Center, Guangzhou 510308, China

[9]Guangzhou Huangpu District Meteorological Bureau, Guangzhou 510530, China

Corresponding authors: Bin Yuan (byuan@jnu.edu.cn)

Table S1. Fitting parameters a and b of different calibration experiments.

Experiment No.	Particle diameter (nm)	Mass loading (ng)	a	b
1	200	150.7	-0.197	1.056
2	200	241	-0.167	1.768
3	200	407	-0.206	3.732
4	100	90.5	-0.218	3.641
5	100	110.6	-0.241	5.229
6	100	150.8	-0.243	4.451

Table S2. The detailed information of three selected periods.

	Periods	Days
Long-range Transport	14-20 October; 29 October-1 November; 3-4 November; 7-10 November; 14 November	18
Urban Air Masses	7-9 October; 23-27 October; 1-2 November; 13 November	11
Coastal Air Masses	2-4 October; 10-12 October; 22 October; 12 November	8

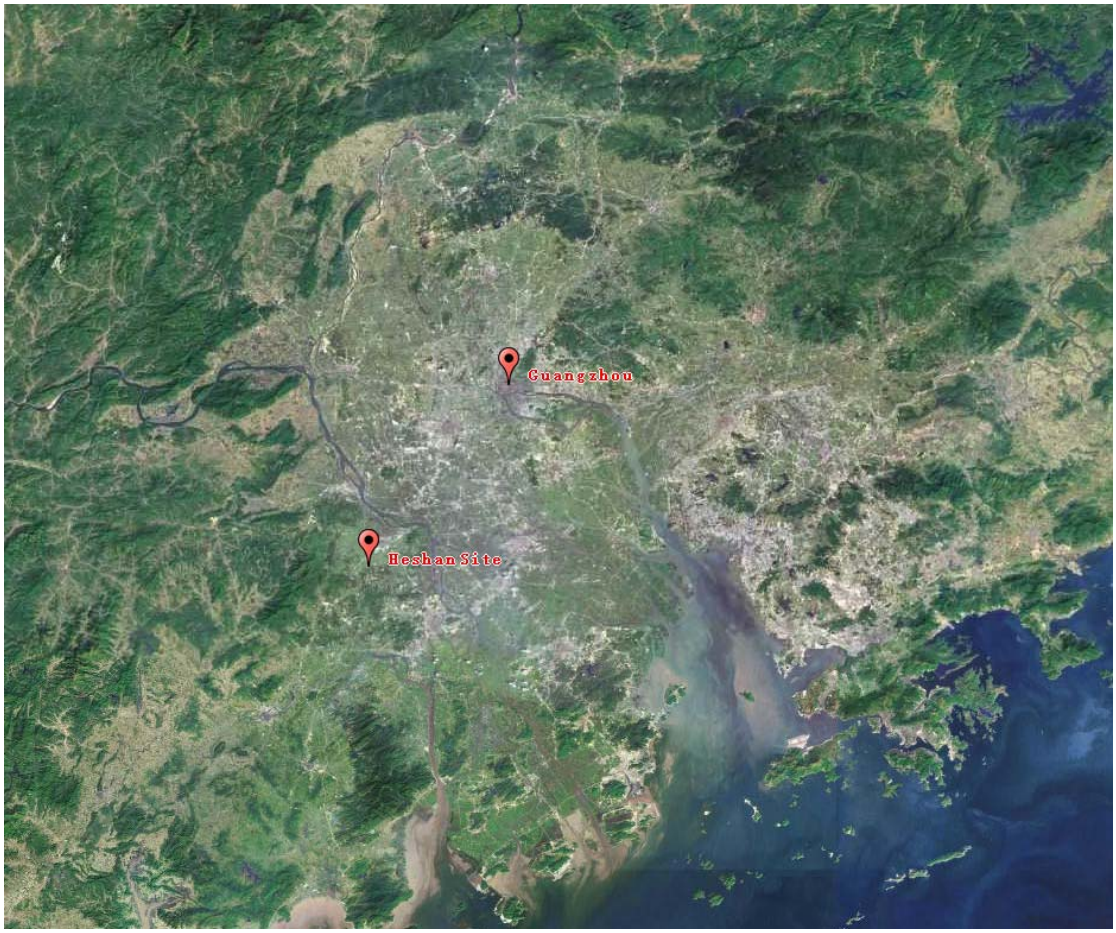

Figure S1. Location of the measurement site and Guangzhou city. This map was obtained from Map World.

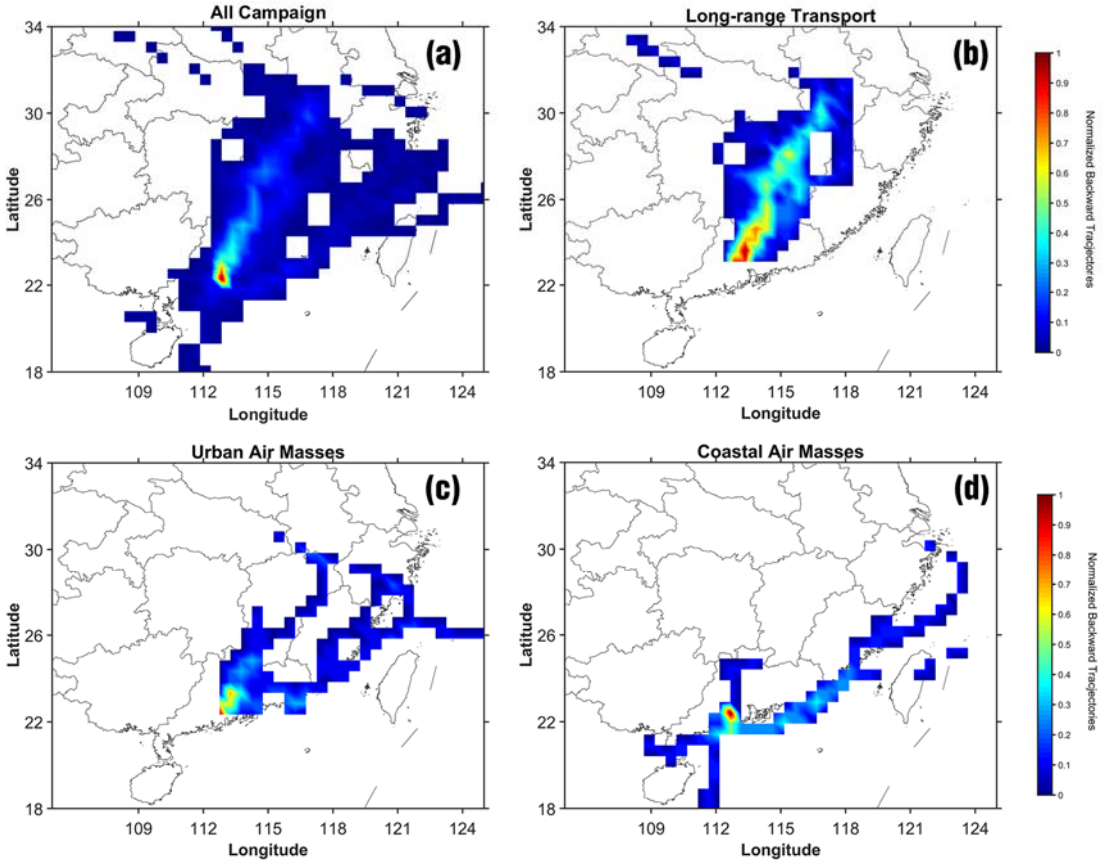

Figure S2. Normalized 72 hours backward trajectories arriving at the measurement site during (a) the whole measurement, (b) long-range transport period, (c) urban air masses period, and (d) coastal air masses period.

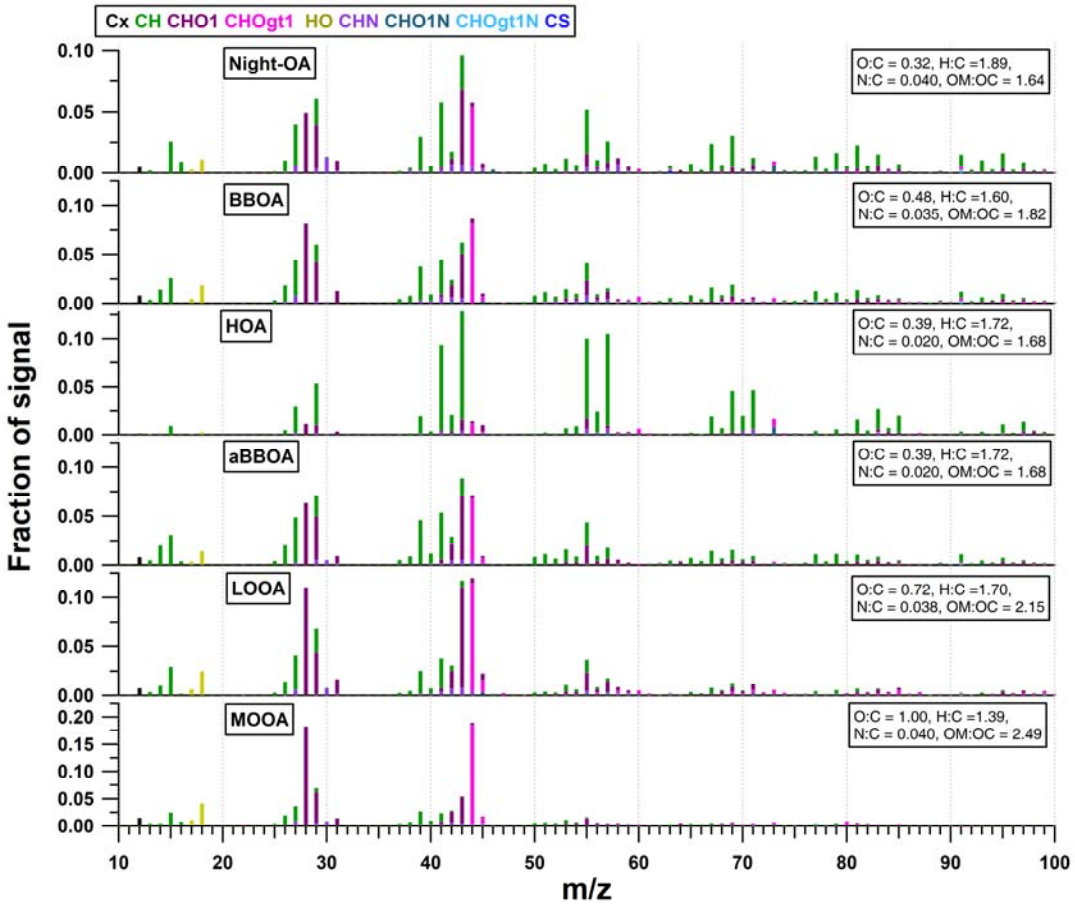

Figure S3. Mass spectral profile of six OA factors. The colors represent different family groups.

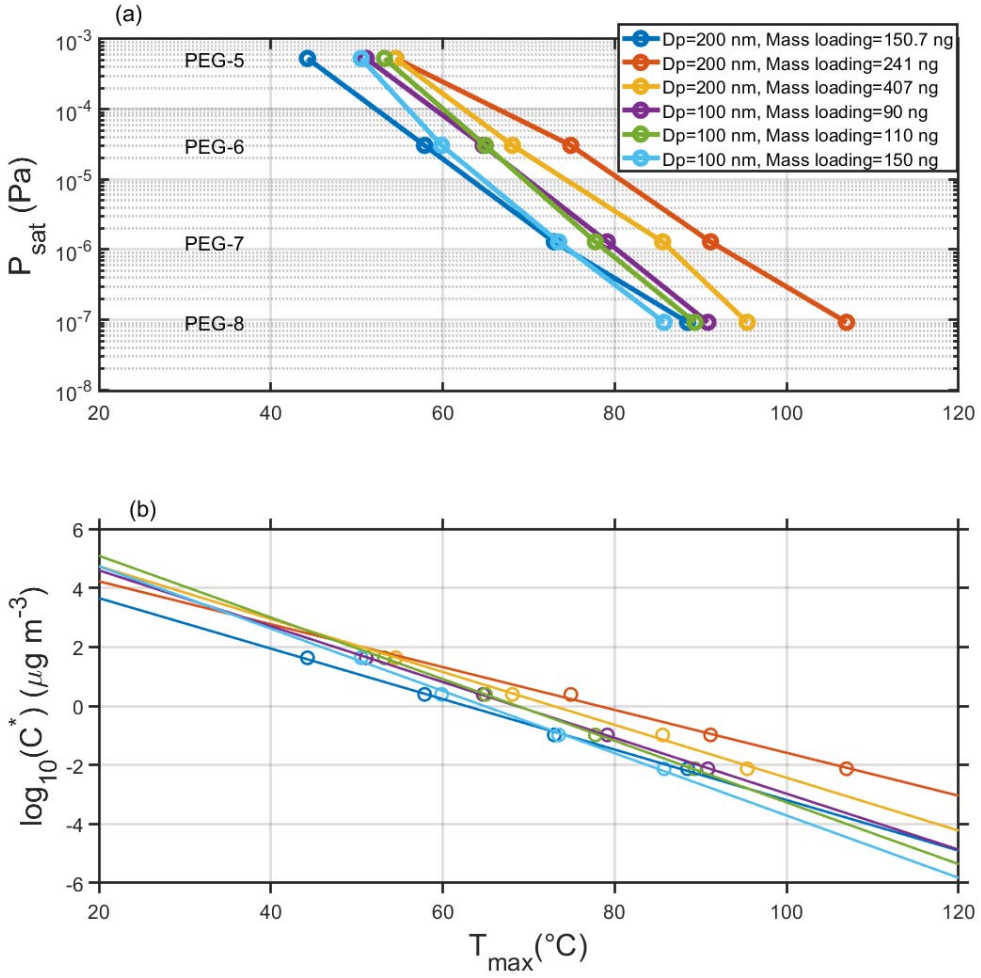

Figure S4. (a) Measured T_{max} vs P_{sat} literature values for PEG 5-8 at different diameters and collected mass loadings and (b) corresponding fitted calibration lines.

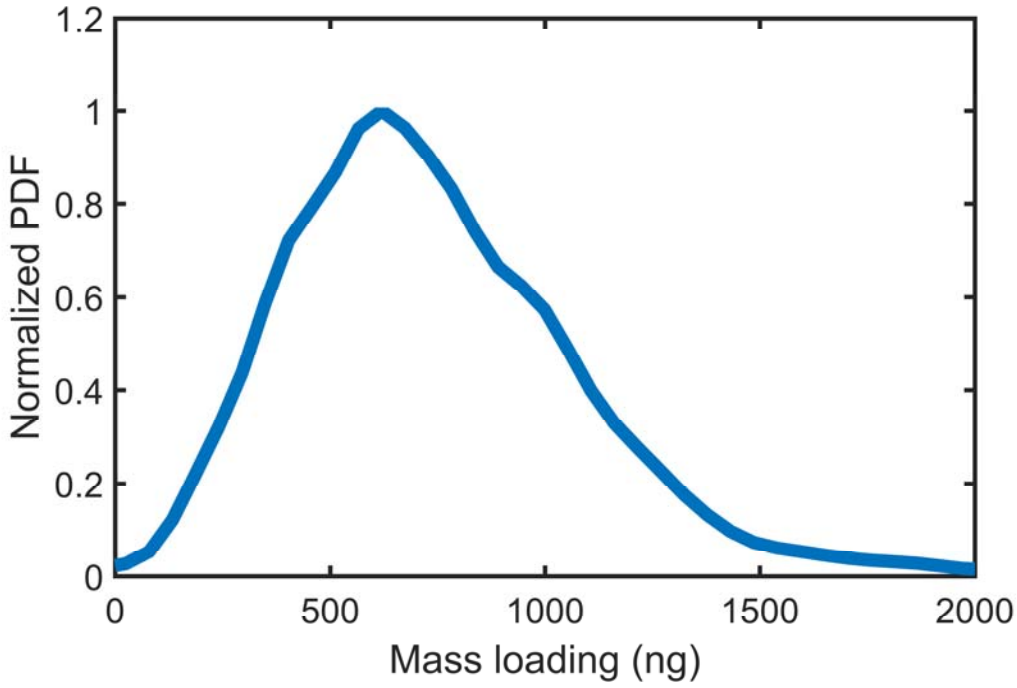

Figure S5. Normalized probability density function of collected mass loading on the filter of the FIGAERO-I-CIMS. The collected mass loading is calculated based on collection time, flow rate through the filter, and the organic concentration measured by the SP-AMS.

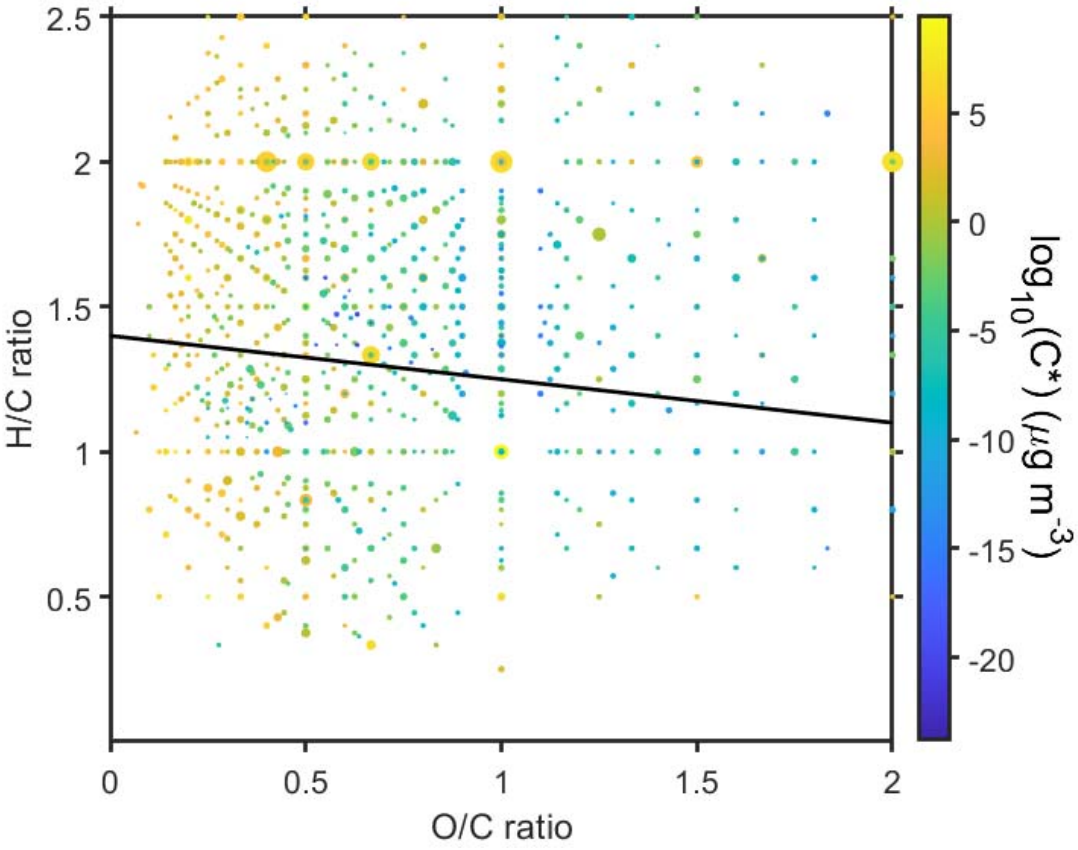

Figure S6. Van-Krevelen diagram (O/C ratio versus H/C ratio) of gas-phase organic compounds measured by FIGAERO-CIMS. The symbol size is proportional to the mass concentration of organic vapors and the color code represents the volatility. The black solid line divided the organic vapors potentially formed through the autoxidation pathway (upper regime) and multi-generation OH oxidation pathway (lower regime)(Wang et al., 2022; Wang et al., 2020).

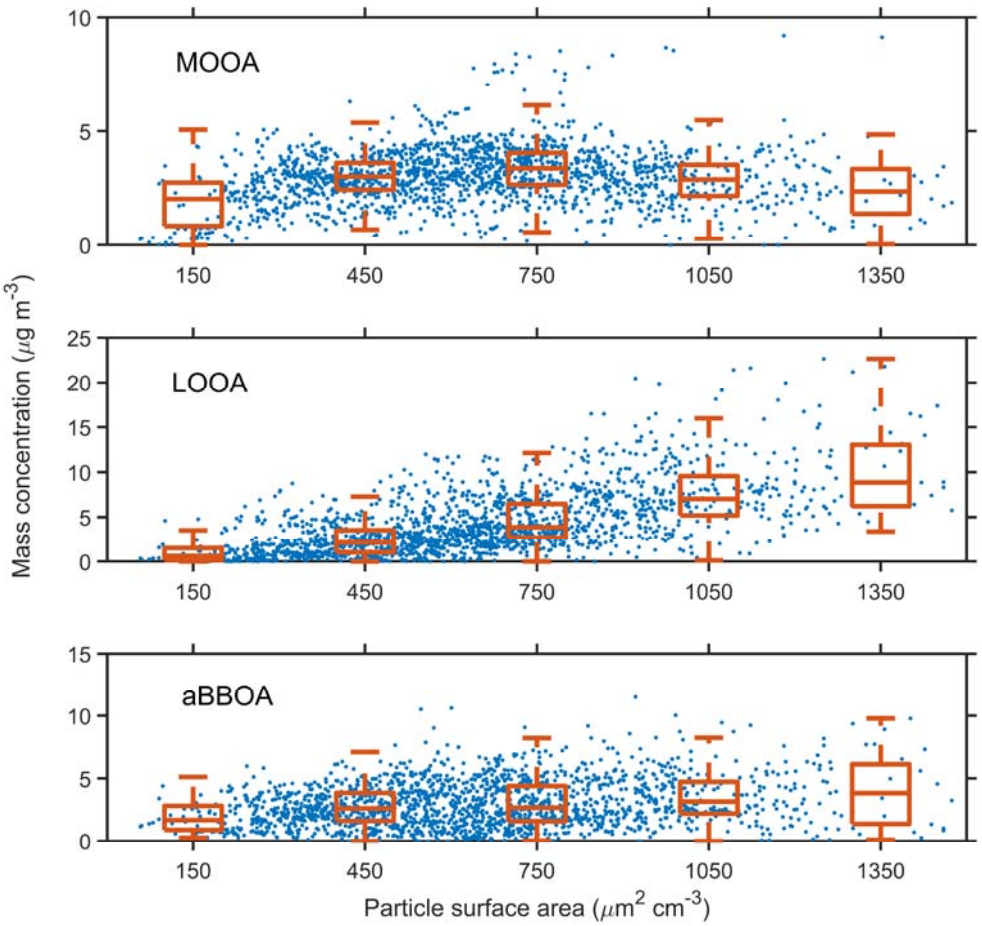

Figure S8. Relationship between particle surface area and SOA factors (MOOA, LOOA and aBBOA).

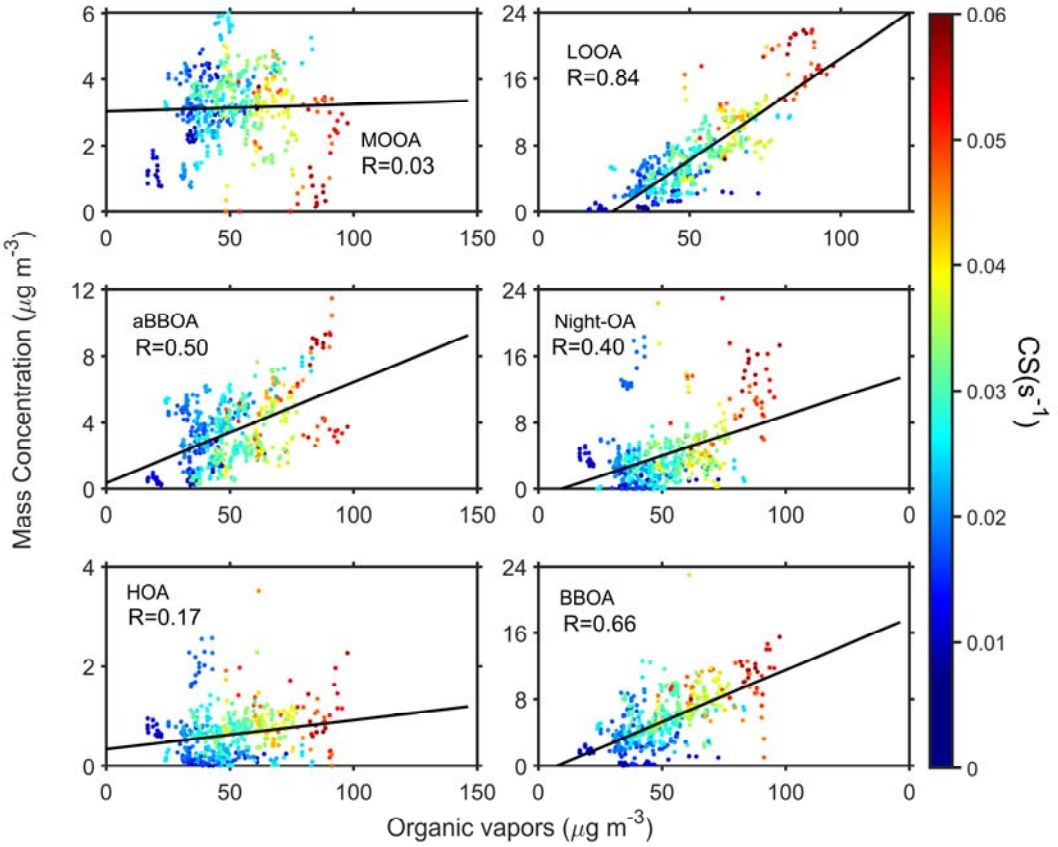

Figure S8. Relationship between the concentration of organic vapors and six OA PMF factors. The color represents the CS values.

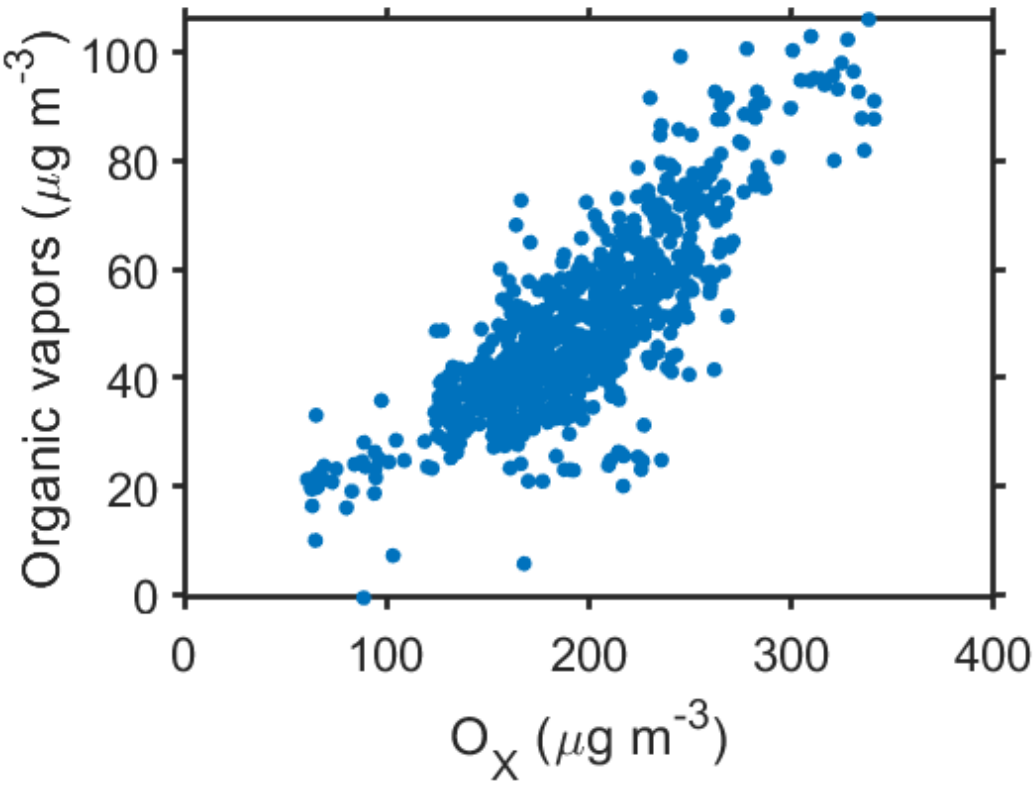

Figure S9. Relationship between odd-oxygen (O_X, O_X=O_3+NO_2) and the concentration of organic vapors measured by the FIGAERO-CIMS in the afternoon (10:00-16:00 LT).

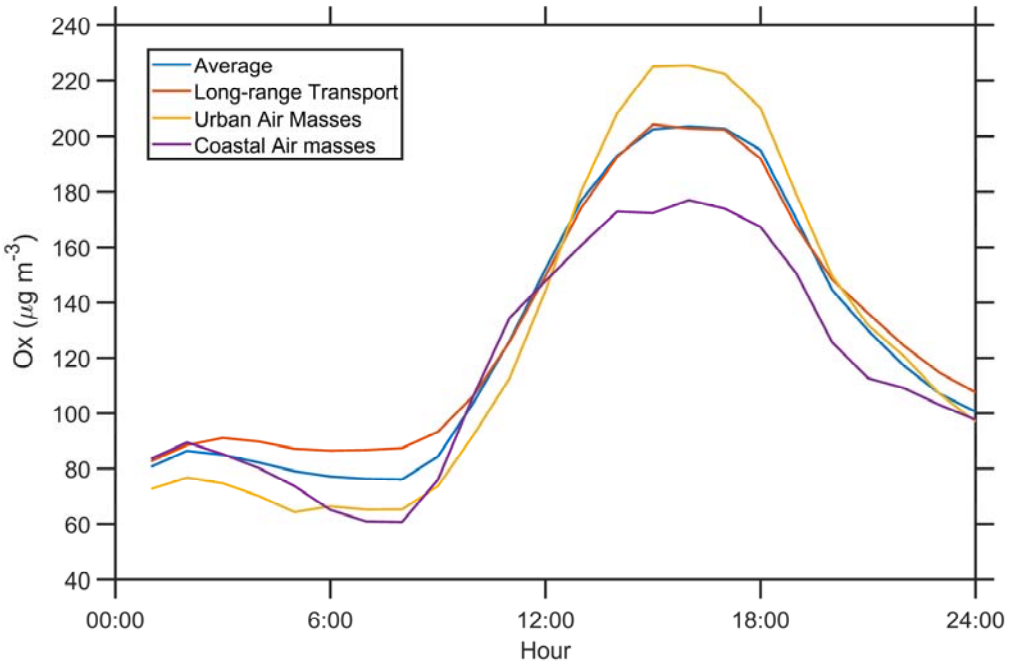

Figure S10. The average diurnal variation of O_x during the whole campaign, long-range transport, urban air masses, and coastal air masses periods.

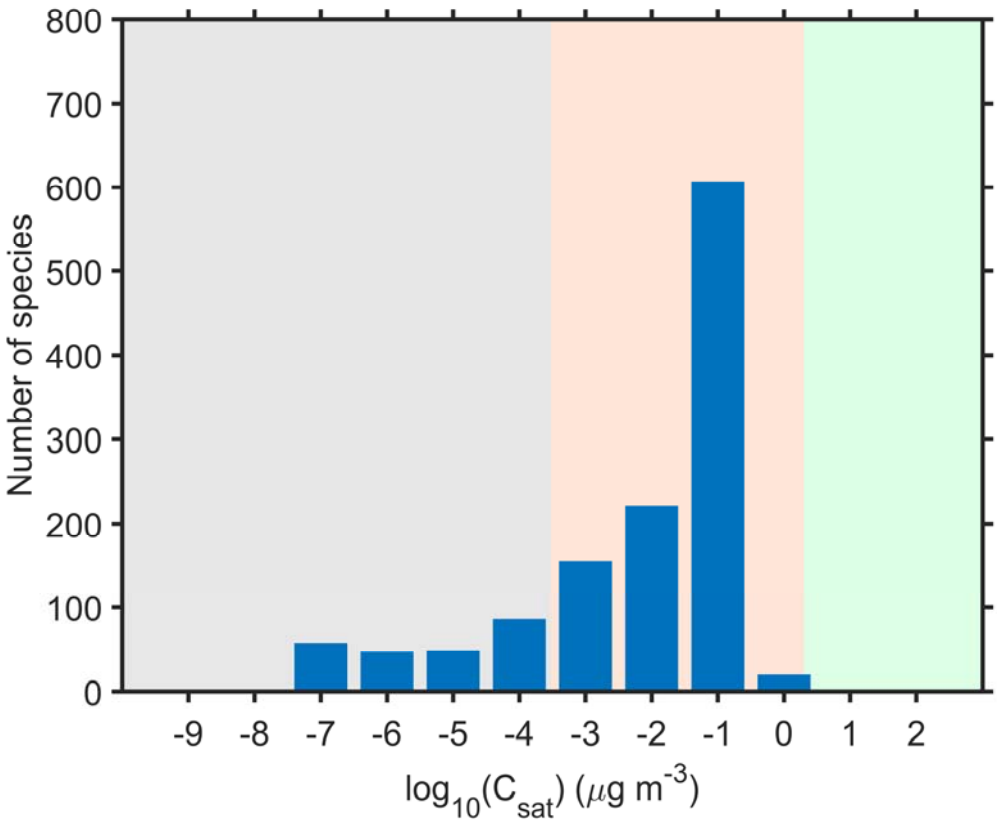

Figure S11. Volatility distribution of the number of calibrated and semi-quantified species measured by the FIGAERO-CIMS.

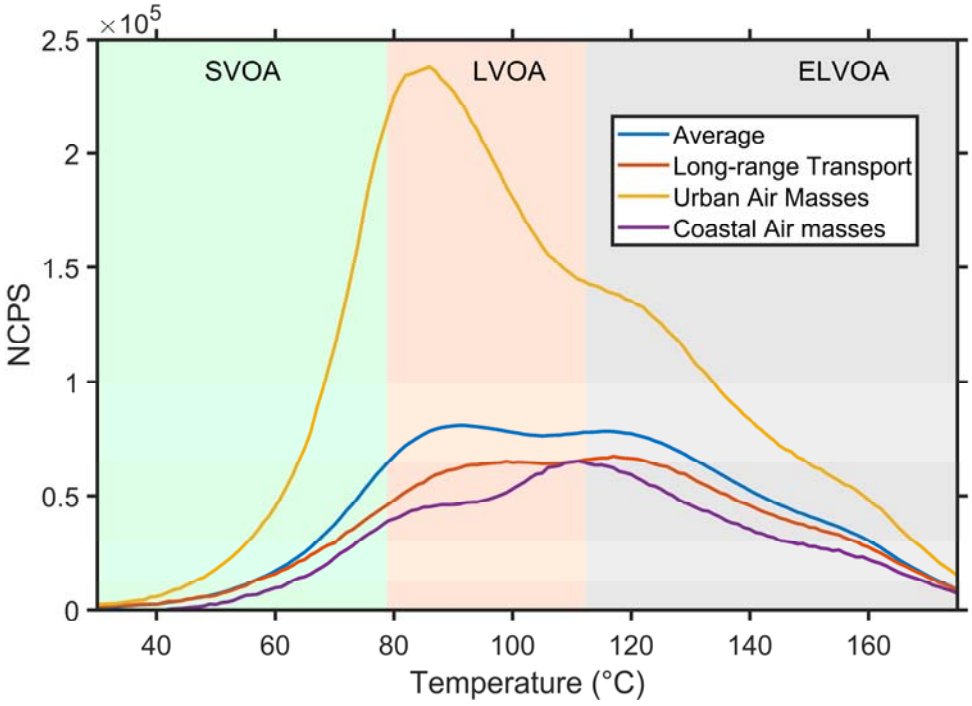

Figure S12. Average sum thermograms measured by the FIGAERO-CIMS in the afternoon (12:00-16:00 LT) during the whole campaign, long-range transport, urban air masses, and coastal air masses periods.

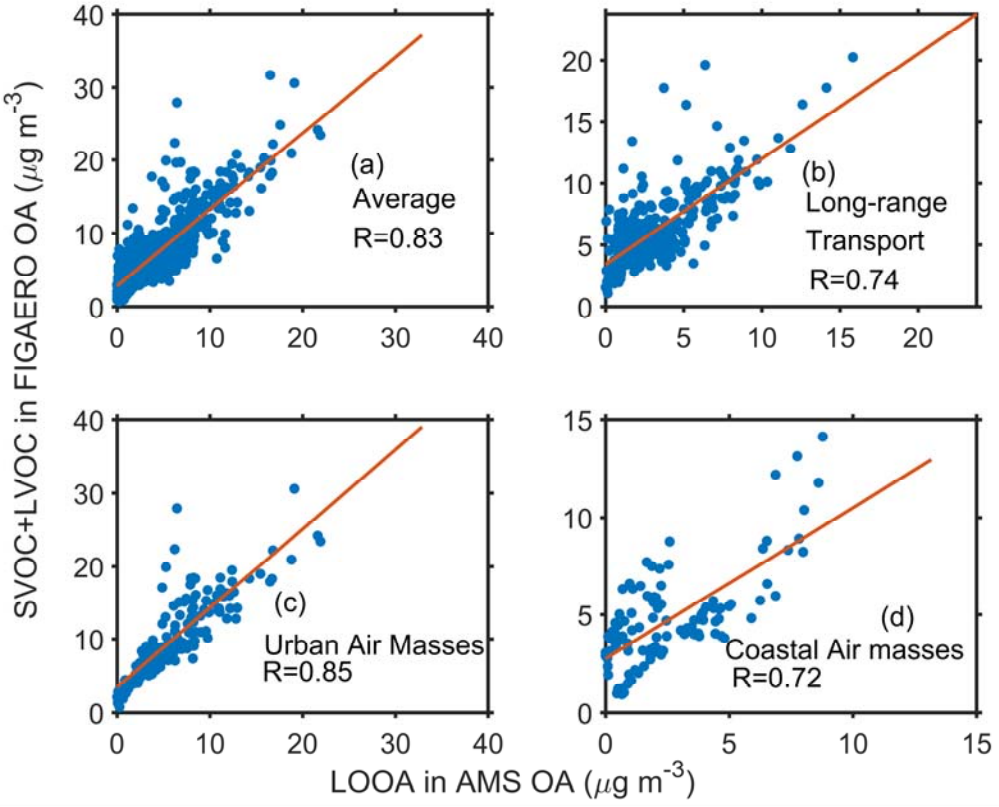

Figure S13. Relationship between the SVOC+LVOC in FIGAERO OA and LOOA in AMS OA during (a) the whole campaign, (b) long-range transport, (c) urban air masses, and (d) coastal air masses periods.

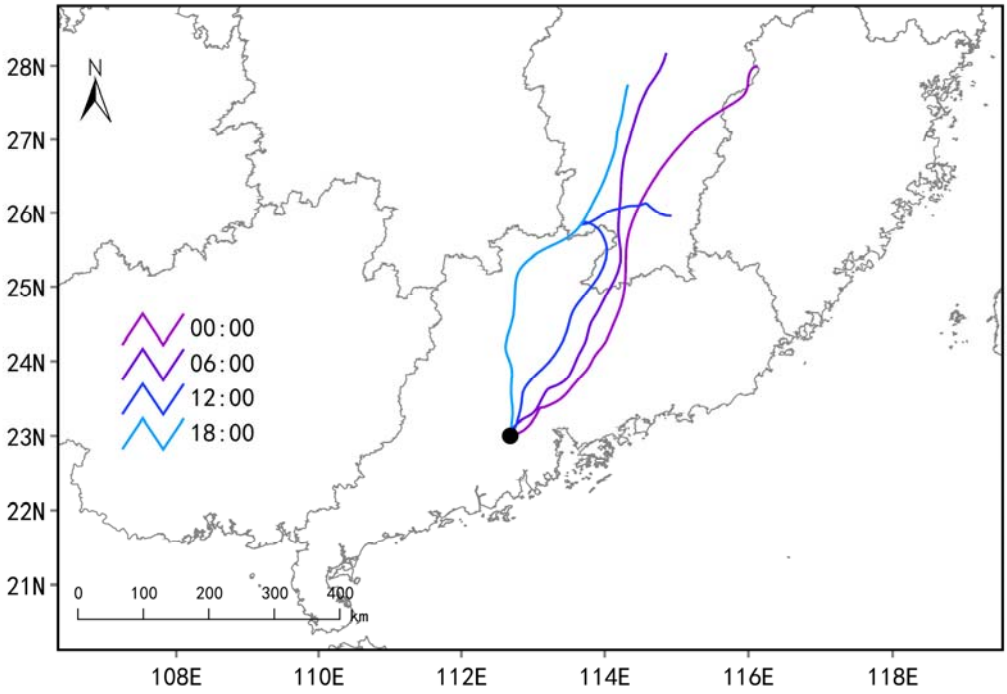

Figure S14. 72h backward trajectories arriving at the measurement site with 500 m height at 00:00, 06:00, 12:00, and 18:00 on 2 November 2019.

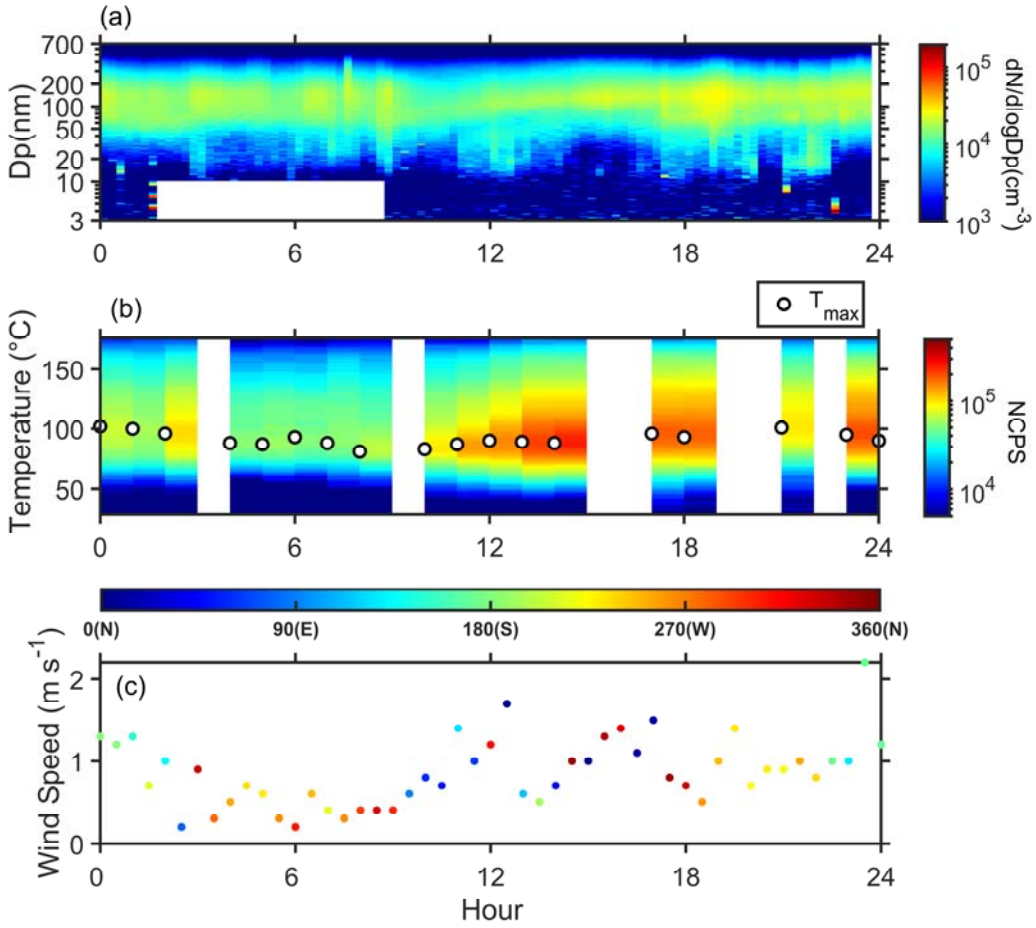

Figure S15. Variation of (a) PNSD, (b) sum thermograms, and (c) wind speed and direction on 2 November 2019.

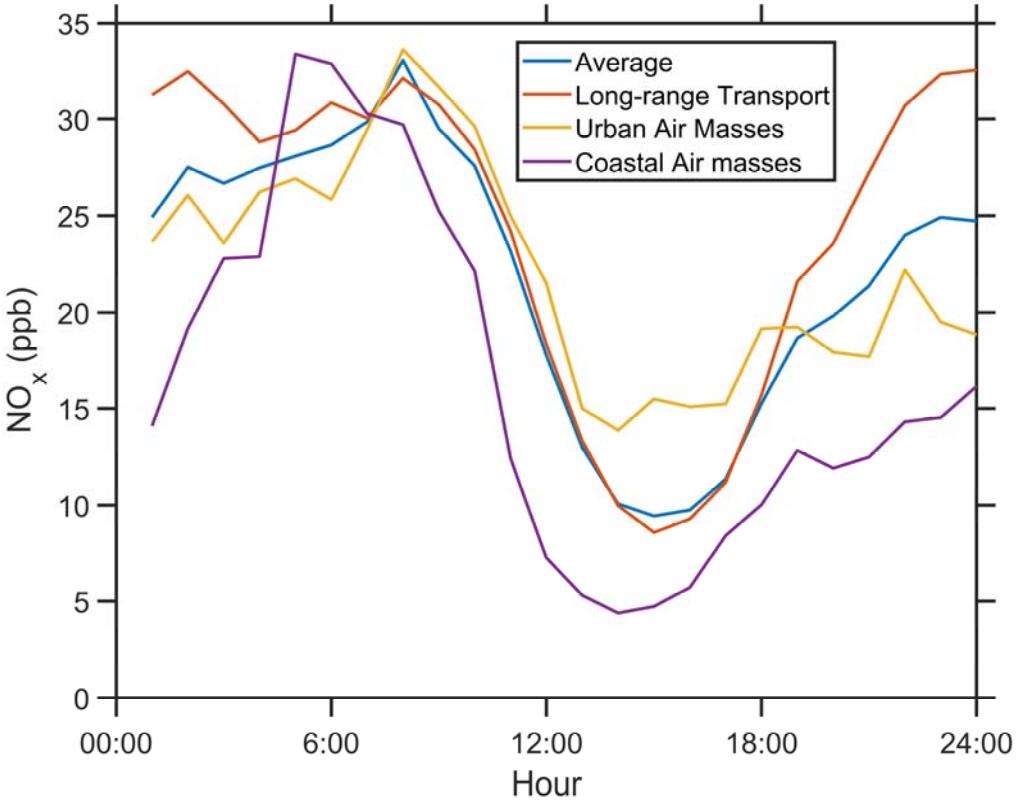

Figure S16. The average diurnal variation of NO_x during the whole campaign and three selected periods.

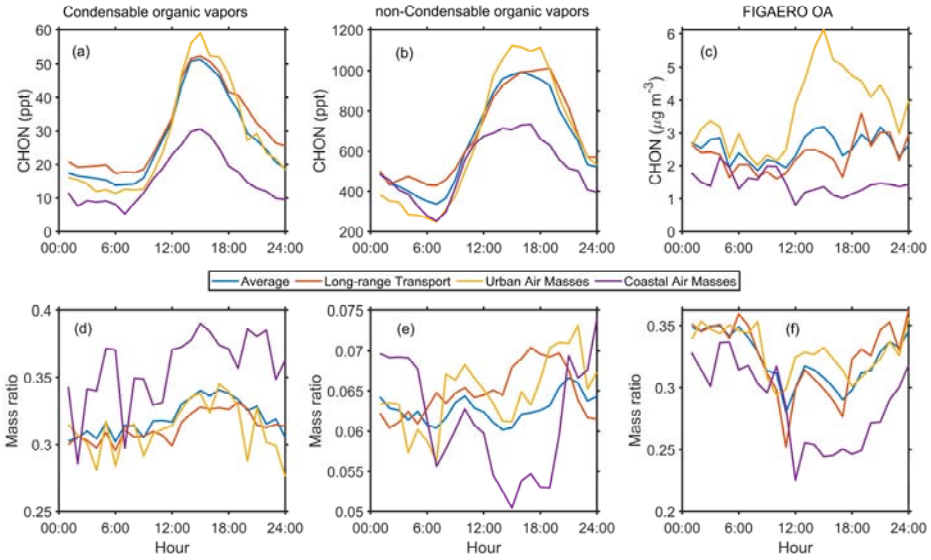

107

108 Figure S17. Diurnal variation of CHON compounds in (a) condensable organic vapors, (b) non-
109 condensable organic vapors, and (c) FIGAERO OA and (d-f) their corresponding mass ratio.

110

References

Wang, M., Chen, D., Xiao, M., Ye, Q., Stolzenburg, D., Hofbauer, V., Ye, P., Vogel, A. L., Mauldin, R. L., Amorim, A., Baccarini, A., Baumgartner, B., Brilke, S., Dada, L., Dias, A., Duplissy, J., Finkenzeller, H., Garmash, O., He, X.-C., Hoyle, C. R., Kim, C., Kvashnin, A., Lehtipalo, K., Fischer, L., Molteni, U., Petäjä, T., Pospisilova, V., Quéléver, L. L. J., Rissanen, M., Simon, M., Tauber, C., Tomé, A., Wagner, A. C., Weitz, L., Volkamer, R., Winkler, P. M., Kirkby, J., Worsnop, D. R., Kulmala, M., Baltensperger, U., Dommen, J., El-Haddad, I., and Donahue, N. M.: Photo-oxidation of Aromatic Hydrocarbons Produces Low-Volatility Organic Compounds, Environmental Science & Technology, 54, 7911-7921, 10.1021/acs.est.0c02100, 2020.

Wang, Y., Clusius, P., Yan, C., Dällenbach, K., Yin, R., Wang, M., He, X.-C., Chu, B., Lu, Y., Dada, L., Kangasluoma, J., Rantala, P., Deng, C., Lin, Z., Wang, W., Yao, L., Fan, X., Du, W., Cai, J., Heikkinen, L., Tham, Y. J., Zha, Q., Ling, Z., Junninen, H., Petäjä, T., Ge, M., Wang, Y., He, H., Worsnop, D. R., Kerminen, V.-M., Bianchi, F., Wang, L., Jiang, J., Liu, Y., Boy, M., Ehn, M., Donahue, N. M., and Kulmala, M.: Molecular Composition of Oxygenated Organic Molecules and Their Contributions to Organic Aerosol in Beijing, Environmental Science & Technology, 56, 770-778, 10.1021/acs.est.1c05191, 2022.